Construction and Building Materials 322 (2022) 126481

Contents lists available at ScienceDirect

Construction and Building Materials

journal homepage: www.elsevier.com/locate/conbuildmat

Moment-resisting beam-to-column timber connections with inclined threaded rods: Structural concept and analysis by use of the component method

Haris Stamatopoulos *, Kjell Arne Malo, Aivars Vilguts

Department of Structural Engineering, Norwegian University of Science and Technology (NTNU), Rich. Birkelandsvei 1A, Trondheim 7491, Norway

ARTICLE INFO

Keywords:
Moment-resisting connection
Threaded rod
Beam
Column
Rotational stiffness

ABSTRACT

The use of moment-resisting frames with semi-rigid connections as a lateral load-carrying system in timber buildings can reduce the need for bracing with diagonal members or walls and allow for more open and flexible architecture. The overall performance of moment-resisting frames depends largely on the properties of their connections. Screwed-in threaded rods with wood screw thread feature high axial stiffness and capacity and they may be used as fasteners in beam-to-column, moment-resisting timber connections. In the present paper, a structural concept for a beam–to-column, moment-resisting timber connection based on threaded rods is presented and explained. Analytical expressions for the estimation of the rotational stiffness and the forces in the rods were derived based on a component-method approach. The analytical predictions for stiffness were compared to experimental results from full scale tests and the agreement was good.

1. Introduction

1.1. Background

WOODSOL is a Norwegian research project which aims to develop a structural system for multi-storey timber buildings based on moment-resisting frames (abbr. MRFs) [1]. The design of multi-storey timber buildings is often governed by the fulfilment of serviceability requirements, namely the restriction of wind-induced accelerations and deflections and human-induced vibrations within acceptable limits. Considering structures subjected to horizontal loading (e.g. wind), MRFs with semi-rigid, beam-to-column, moment-resisting connections as a lateral load-carrying system, can reduce the need for bracing with diagonal members or walls and therefore allow for more open and flexible architecture. Recent studies [2,3] have shown that a minimum rotational stiffness of connections of the order of 10000–15000 kNm/rad is required in multi-storey MRFs, in order to fulfil the serviceability requirements due to wind-induced deflections and accelerations. With respect to human-induced vibrations, rotationally stiff connections at the ends of beams and floors may significantly improve their performance [3,4] allowing for longer spans. Moreover, MRFs are statically indeterminate structures and the distribution of internal forces and moments at the Ultimate Limit State, depend on the rotational stiffness of their connections. Therefore, the overall performance of MRFs depends largely on their connections and an accurate estimation of the rotational stiffness is necessary in the analysis of MRFs.

Compared to axially loaded fasteners, laterally loaded fasteners feature lower stiffness. Consequently, in order to achieve the required rotational stiffness in connections with laterally loaded fasteners, a large number of fasteners and shear planes may be required. In the literature, analytical models and experimental results for moment-resisting connections with axially loaded fasteners can be found, mainly for two types of fasteners: inclined self-tapping screws, see e.g. [5–7] and glued-in rods inserted parallel or perpendicular to grain, see e.g. [8–10]. Axially loaded threaded rods (i.e. screwed-in rods with wood-screw threads) can be a promising alternative for such connections as they feature high axial capacity and stiffness [11,12]. To achieve a fast and economic assembly, it is better to pre-install threaded rods and coupling parts in the beam and the column and only do mounting of the coupling parts at the building site. The mounting between the parts at the building site, should be simple, reliable and should not influence the stiffness of the connection.

* Corresponding author.
E-mail address: haris.stamatopoulos@ntnu.no (H. Stamatopoulos).

https://doi.org/10.1016/j.conbuildmat.2022.126481
Received 3 November 2021; Received in revised form 12 January 2022; Accepted 13 January 2022
Available online 19 January 2022

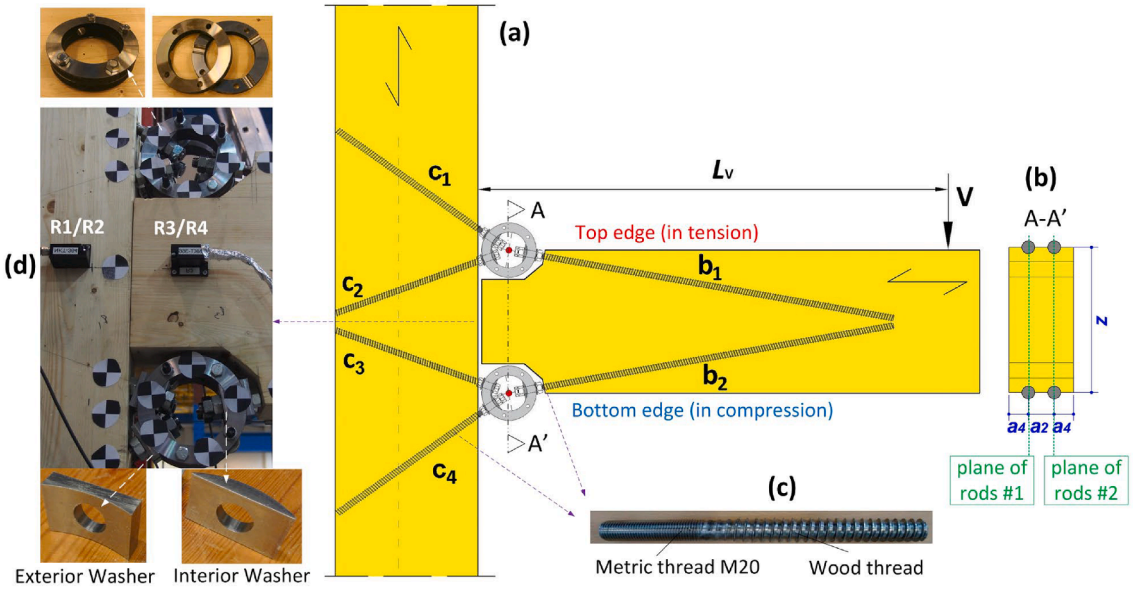

Fig. 1. Moment-resisting, beam-to-column timber connection with threaded rods: (a) lay-out of structural concept, (b) section view, (c) threaded rods with wood screw thread and metric thread at their end, (d) details of the fastening of the threaded rods to the steel ring couplers.

1.2. Outline

A structural concept for a moment-resisting, beam-to-column, timber connection is presented and explained in this paper. The concept is based on threaded rods which are mainly axially loaded, to take advantage of their high axial stiffness and capacity. Focus is given on the derivation and formulation of analytical expressions for the rotational stiffness and the forces in the rods since these are important inputs in the analysis and the design process. The analytical predictions are compared to experimental results from full-scale tests of prototype, moment-resisting connections between glued-laminated timber (abbr. glulam) members.

2. Conceptual design of connection

2.1. General remarks

The structural concept for a moment-resisting, beam-to-column timber connection with inclined threaded rods is presented in Fig. 1. The rods are inserted in pre-drilled holes in the beam and the column and jointed by use of coupling parts. In the study [13] which is used here to illustrate the concept, purpose-made steel rings were used as the coupling parts, see Fig. 1(d). To allow fastening of rods to the rings, threaded rods with metric thread at their end are used, confer Fig. 1(c). A great challenge in beam-to-column moment-resisting connections is the transfer of forces between two members whose grain orientation differs by 90 degrees. Wood is 15–30 times stiffer along the grain compared to transversal directions. To utilize the higher material stiffness of wood parallel to grain, loading perpendicular to grain should be minimized. Moreover, threaded rods are optimized for axial loading and therefore lateral loading of the rods should be minimized to fully utilize their potential. Axially loaded rods are very stiff fasteners especially when they are installed with small inclination to the grain direction and they allow for immediate load take-up, without initial slip [12].

2.2. Column-side connection

The coupling parts are connected to the column by use of a pair of inclined threaded rods in each side (rods c_1-c_2 at the top and rods c_3-c_4 at the bottom), see Fig. 1(a). Due to the inclination of the rods and the existence of shear forces, a load situation consisting of both axial and lateral forces occurs in the rods. However, the rods will mainly experience axial forces since their axial stiffness is much greater than the lateral one. The transfer of forces in this configuration resembles the transfer of forces in a truss, where members are predominantly axially loaded. Therefore, the lateral forces in the threaded rods c_1, c_2, c_3 and c_4 may be neglected. Wood is very soft perpendicular to grain and transfer of forces by contact between the column and the coupling part at the compressive side would result in low contribution to the overall stiffness. Moreover, transfer of forces by contact may be influenced by potential shrinkage of the timber members. Therefore, transfer of forces by contact is neglected and the compressive forces are assumed to be transferred only by the threaded rods.

2.3. Beam-side connection

Threaded rods oriented parallel to the grain are vulnerable to cracks since a single crack along the grain might lead to a considerable loss of strength if the crack occurs in the same plane as the rod. Therefore, the beam is connected to the coupling parts by use of threaded rods (b_1 and b_2) inserted at a small angle to the grain, i.e. 5–10 deg, see Fig. 1(a). Greater angle is avoided, as it would also result in high lateral forces in the threaded rods and therefore smaller stiffness. Moreover, a small inclination of the rods on the beam side allows for increased penetration length and higher axial stiffness of the rods. Installing the threaded rods with a small inclination, allows also to install them with very small (even zero) edge distance, resulting in increased lever arm and therefore in increased moment resistance and rotational stiffness, see Fig. 1(a and b). This is an advantage of inclined rods compared to either rods inserted parallel to grain or laterally loaded fasteners.

2.4. Metallic coupling parts

The inclination of rods gives some practical implications in jointing the different parts. The use of steel rings as coupling parts gives the opportunity to insert threaded rods in different angles to the grain and join them in one point; in this way eccentricities are avoided. Purpose-made washers are used to fasten the threaded rods in the rings with nuts, see Fig. 1(d). To allow the assembly of the connection, the rings are sliced in the symmetry line resulting in two parts, wrapped around the

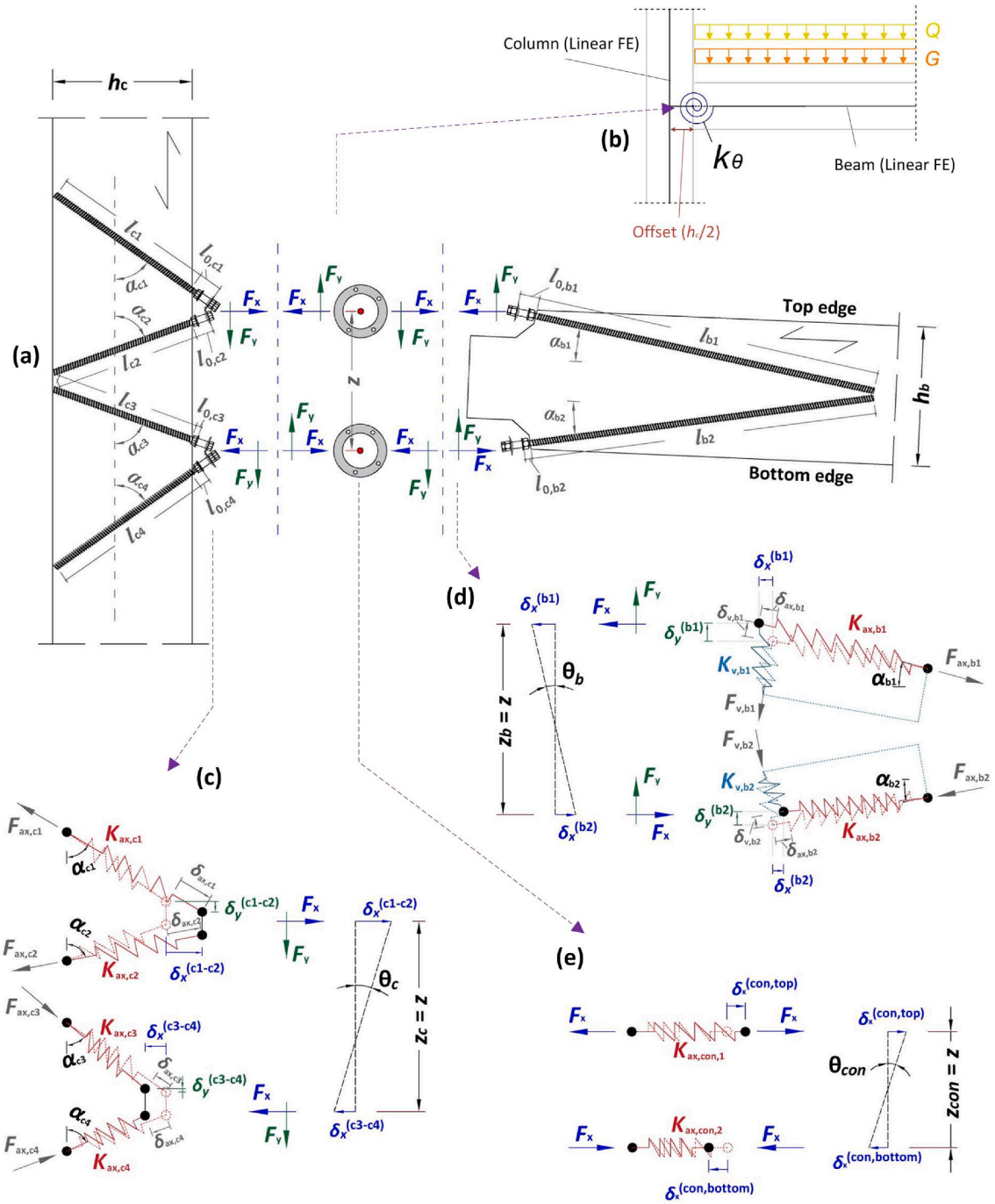

Fig. 2. Component method: (a) Acting forces on each part of the connection, (b) Finite Element model of the connection, (c)-(e) Components, forces and displacements at the column side (c), at the beam side (d) and in the steel coupling parts (e) (dashed lines: initial position of springs).

rods and fastened together with bolts, see Fig. 1(d). Beam-to-column connections are typically subjected to alternating moment due to wind or earthquake loading. To transfer forces both in tension and compression due to alternating loading, special washers and nuts are placed both in the interior and the exterior surface of the coupling rings, see the detail in Fig. 1(d).

3. Component method

3.1. Spring components and force distribution

Fig. 2(a) shows the acting forces on each part of the connection, due to moment-loading as shown in Fig. 1(a). The analysis presented in this Section is for each plane of rods, i.e. rods inserted at the same plane. Each rod is represented by two linear-elastic springs taking into account their axial stiffness $K_{ax,i}$ and their lateral stiffness $K_{v,i}$. No contact is assumed between the beam and the column or between steel rings and timber members. The distance between the centroids of the steel rings is denoted z, see Fig. 2(a). Note that in the concept in Fig. 1 the rods are connected concentrically in the rings and thus the distance z is the same for all parts of the connection, i.e. $z = z_{beam} = z_{column} = z_{con}$. The following abbreviations are used for the sine and the cosine values of the angles of the rods to the grain direction in the column (α_{ci}) and in the beam (α_{bi}):

$$s_{ci} = \sin(\alpha_{ci}); c_{ci} = \cos(\alpha_{ci}); s_{bi} = \sin(\alpha_{bi}); c_{bi} = \cos(\alpha_{bi}); \quad (1)$$

In FE models, the beams and the columns are typically modelled as linear finite elements (located at the centroids of the elements). The connection can be modelled by a rotational spring. To take into account the fact that the beam is not continuous, it is convenient to model the rotational spring located at the edge of the column, with an offset to the centroid of the column, as shown in Fig. 2(b). Based on this modelling approach, moment is determined at the edge of the column in the present paper.

The magnitude of the horizontal force F_x per plane of rods is obtained by equilibrium (see Fig. 2(a)):

$$F_x = \frac{1}{n} \bullet \frac{M}{z} \quad (2)$$

As an approximation, it is assumed that the shear force is equally distributed between the top and the bottom edge, i.e.:

$$F_y \approx \frac{1}{n} \bullet \frac{V}{2} = \frac{1}{n} \bullet \frac{M}{2 \bullet L_v} \quad (3)$$

where L_v is the lever arm (see Fig. 1(a)) and n is the number of planes of rods, see also Fig. 1(b).

3.2. Stiffness and forces in each rod

3.2.1. Column-side connection

The components, the forces, and the displacements of the connection between the steel coupling parts and the column are shown in Fig. 2(c). The axial stiffness $K_{ax,ci}$ of threaded rods is much greater than their lateral stiffness $K_{v,ci}$, i.e. $K_{ax,ci} \gg K_{v,ci}$, and since two rods are used to connect each coupling part to the column (rods c_1 and c_2 at the top and rods c_3 and c_4 at the bottom), forces are mainly transferred in the axial direction of the rods. Therefore, the lateral springs may be neglected in this case. In fact, the following analysis considering lateral springs leads to similar results but much more cumbersome expressions.

Eqs. (4) and (5) provide the forces-displacements relation in the global coordinate system at the tensile side (rods c_1-c_2) and the compressive side (rods c_3-c_4), according to the component model in Fig. 2(c). As indicated by Eqs. (4) and (5), linear elasticity is assumed in the rods.

$$\begin{Bmatrix} F_x \\ F_y \end{Bmatrix}^{(c1-c2)} = \boldsymbol{Q}_{e,12}{}^{T} \bullet \begin{bmatrix} K_{ax,c1} & 0 \\ 0 & K_{ax,c2} \end{bmatrix} \bullet \boldsymbol{Q}_{e,12} \bullet \begin{Bmatrix} \delta_x \\ \delta_y \end{Bmatrix}^{(c1-c2)} \quad (4)$$

$$\begin{Bmatrix} F_x \\ F_y \end{Bmatrix}^{(c3-c4)} = \boldsymbol{Q}_{e,34}{}^{T} \bullet \begin{bmatrix} K_{ax,c3} & 0 \\ 0 & K_{ax,c4} \end{bmatrix} \bullet \boldsymbol{Q}_{e,34} \bullet \begin{Bmatrix} \delta_x \\ \delta_y \end{Bmatrix}^{(c3-c4)} \quad (5)$$

$\boldsymbol{Q}_{e,12}$ and $\boldsymbol{Q}_{e,34}$ are the transformation matrices given by Eq. (6):

$$\boldsymbol{Q}_{e,12} = \begin{bmatrix} s_{c1} & c_{c1} \\ s_{c2} & -c_{c2} \end{bmatrix}; \boldsymbol{Q}_{e,34} = \begin{bmatrix} s_{c3} & c_{c3} \\ s_{c4} & -c_{c4} \end{bmatrix} \quad (6)$$

Solving Eqs. (4) and (5) for the displacements in the global coordinate system results in Eqs. (7) and (8):

$$\begin{Bmatrix} \delta_x \\ \delta_y \end{Bmatrix}^{(c1-c2)} = \begin{bmatrix} S_{xx,c} & -S_{xy,c} \\ -S_{xy,c} & S_{yy,c} \end{bmatrix}^{(c1-c2)} \bullet \begin{Bmatrix} F_x \\ F_y \end{Bmatrix}^{(c1-c2)} \quad (7)$$

$$\begin{Bmatrix} \delta_x \\ \delta_y \end{Bmatrix}^{(c3-c4)} = \begin{bmatrix} S_{xx,c} & -S_{xy,c} \\ -S_{xy,c} & S_{yy,c} \end{bmatrix}^{(c3-c4)} \bullet \begin{Bmatrix} F_x \\ F_y \end{Bmatrix}^{(c3-c4)} \quad (8)$$

The compliance terms in Eqs. (7) and (8) are given by the following expressions:

$$S_{xx,c}{}^{(c1-c2)} = \frac{\frac{s_{c1}{}^2}{K_{ax,c2}} + \frac{c_{c2}{}^2}{K_{ax,c1}}}{(c_{c1} \bullet s_{c2} + c_{c2} \bullet s_{c1})^2}; S_{xx,c}{}^{(c3-c4)} = \frac{\frac{s_{c3}{}^2}{K_{ax,c4}} + \frac{c_{c4}{}^2}{K_{ax,c3}}}{(c_{c3} \bullet s_{c4} + c_{c4} \bullet s_{c3})^2} \quad (9)$$

$$S_{yy,c}{}^{(c1-c2)} = \frac{\frac{s_{c1}{}^2}{K_{ax,c2}} + \frac{s_{c2}{}^2}{K_{ax,c1}}}{(c_{c1} \bullet s_{c2} + c_{c2} \bullet s_{c1})^2}; S_{yy,c}{}^{(c3-c4)} = \frac{\frac{s_{c3}{}^2}{K_{ax,c4}} + \frac{s_{c4}{}^2}{K_{ax,c3}}}{(c_{c3} \bullet s_{c4} + c_{c4} \bullet s_{c3})^2} \quad (10)$$

$$S_{xy,c}{}^{(c1-c2)} = \frac{\frac{c_{c1} \bullet s_{c1}}{K_{ax,c2}} - \frac{c_{c2} \bullet s_{c2}}{K_{ax,c1}}}{(c_{c1} \bullet s_{c2} + c_{c2} \bullet s_{c1})^2}; S_{xy,c}{}^{(c3-c4)} = \frac{\frac{c_{c3} \bullet s_{c3}}{K_{ax,c4}} - \frac{c_{c4} \bullet s_{c4}}{K_{ax,c3}}}{(c_{c3} \bullet s_{c4} + c_{c4} \bullet s_{c3})^2} \quad (11)$$

The forces at the tensile side (rods c_1-c_2) and the compressive side of the connection (rods c3-c4) per plane of rods are given by Eqs. (12) and (13), see also Eqs. (2) and (3) and Fig. 2(a):

$$\begin{Bmatrix} F_x \\ F_y \end{Bmatrix}^{(c1-c2)} = \frac{1}{n} \bullet \begin{Bmatrix} M/z \\ V/2 \end{Bmatrix} = \frac{1}{n} \bullet \begin{Bmatrix} M/z \\ M/(2 \bullet L_v) \end{Bmatrix} \quad (12)$$

$$\begin{Bmatrix} F_x \\ F_y \end{Bmatrix}^{(c3-c4)} = \frac{1}{n} \bullet \begin{Bmatrix} -M/z \\ V/2 \end{Bmatrix} = \frac{1}{n} \bullet \begin{Bmatrix} -M/z \\ M/(2 \bullet L_v) \end{Bmatrix} \quad (13)$$

The horizontal displacements are obtained by substituting Eqs. (12) and (13) into Eqs. (7) and (8):

$$\delta_x{}^{(c1-c2)} = \frac{1}{n} \bullet \left(S_{xx,c}{}^{(c1-c2)} \bullet \frac{M}{z} - S_{xy,c}{}^{(c1-c2)} \bullet \frac{M}{2 \bullet L_v} \right) \quad (14)$$

$$\delta_x{}^{(c3-c4)} = \frac{1}{n} \bullet \left(-S_{xx,c}{}^{(c3-c4)} \bullet \frac{M}{z} - S_{xy,c}{}^{(c3-c4)} \bullet \frac{M}{2 \bullet L_v} \right) \quad (15)$$

The rotation is given as function of the horizontal displacements by Eq. (16), confer also Fig. 2(c):

$$\theta_c = \frac{\delta_x{}^{(c1-c2)} - \delta_x{}^{(c3-c4)}}{z} \quad (16)$$

Combining Eqs. (14) to (16), the rotational stiffness per plane of rods is obtained:

$$K_{\theta,c} = \frac{1}{n} \bullet \frac{M}{\theta_c} = \frac{z^2}{\left(S_{xx,c}{}^{(c1-c2)} + S_{xx,c}{}^{(c3-c4)} \right) + \left(S_{xy,c}{}^{(c3-c4)} - S_{xy,c}{}^{(c1-c2)} \right) \bullet \frac{z}{2 \bullet L_v}} \quad (17)$$

Finally, the axial forces in the rods are given by Eqs. (18) and (19):

$$\begin{Bmatrix} F_{ax,c1} \\ F_{ax,c2} \end{Bmatrix} = \left(\boldsymbol{Q}_{e,12}{}^{T} \right)^{-1} \bullet \begin{Bmatrix} F_x \\ F_y \end{Bmatrix}^{(c1-c2)} = \frac{1}{n} \bullet \begin{Bmatrix} c_{c2} + s_{c2} \bullet z/(2 \bullet L_v) \\ c_{c1} \bullet s_{c2} + c_{c2} \bullet \end{Bmatrix} s_{c1} \frac{c_{c1} - s_{c1} \bullet z/(2 \bullet L_v)}{c_{c1} \bullet s_{c2} + c_{c2} \bullet} s_{c1} \bullet \frac{M}{z} \quad (18)$$

$$\begin{Bmatrix} F_{ax,c3} \\ F_{ax,c4} \end{Bmatrix} = \left(\boldsymbol{Q}_{c,34}{}^{T}\right)^{-1} \bullet \begin{Bmatrix} \mathrm{F_x} \\ \mathrm{F_y} \end{Bmatrix}^{(c3-c4)} = -\frac{1}{\mathrm{n}} \bullet \begin{Bmatrix} \frac{\mathrm{c_{c4}} - \mathrm{s_{c4}} \bullet \mathrm{z}/(2 \bullet \mathrm{L_v})}{\mathrm{c_{c3}} \bullet \mathrm{s_{c4}} + \mathrm{c_{c4}} \bullet} \mathrm{s_{c3}} & \frac{\mathrm{c_{c3}} + \mathrm{s_{c3}} \bullet \mathrm{z}/(2 \bullet \mathrm{L_v})}{\mathrm{c_{c3}} \bullet \mathrm{s_{c4}} + \mathrm{c_{c4}} \bullet} \mathrm{s_{c3}} \end{Bmatrix} \bullet \frac{\mathrm{M}}{\mathrm{z}} \tag{19}$$

3.2.2. Beam-side connection

The components, the forces, and the displacements in the connection between the coupling parts and the beam are shown in Fig. 2(d). The direction of the resultant force does not coincide with the axis of the rod and here it is necessary to consider both the axial ($K_{ax,bi}$) and the lateral stiffness of the rods ($K_{v,bi}$). Eqs. (20) and (21) provide the forces-displacements relations in global coordinates at the tensile (rod b_1) and the compressive side (rod b_2). As indicated by Eqs. (20) and (21), linear and un-coupled elasticity of the rods is assumed.

$$\begin{Bmatrix} F_x \\ F_y \end{Bmatrix}^{(b1)} = \boldsymbol{Q_{b1}}^{T} \bullet \begin{bmatrix} \mathrm{K_{ax,b1}} & 0 \\ 0 & \mathrm{K_{v,b1}} \end{bmatrix} \bullet \boldsymbol{Q_{b1}} \bullet \begin{Bmatrix} \delta_x \\ \delta_y \end{Bmatrix}^{(b1)} \tag{20}$$

$$\begin{Bmatrix} F_x \\ F_y \end{Bmatrix}^{(b2)} = \boldsymbol{Q_{b2}}^{T} \bullet \begin{bmatrix} \mathrm{K_{ax,b2}} & 0 \\ 0 & \mathrm{K_{v,b2}} \end{bmatrix} \bullet \boldsymbol{Q_{b2}} \bullet \begin{Bmatrix} \delta_x \\ \delta_y \end{Bmatrix}^{(b2)} \tag{21}$$

$\boldsymbol{Q_{b1}}$ and $\boldsymbol{Q_{b2}}$ are the transformation matrices given by Eq. (22):

$$\boldsymbol{Q_{b1}} = \begin{bmatrix} c_{b1} & s_{b1} \\ -s_{b1} & c_{b1} \end{bmatrix}; \boldsymbol{Q_{b2}} = \begin{bmatrix} c_{b2} & -s_{b2} \\ s_{b2} & c_{b2} \end{bmatrix} \tag{22}$$

Solving Eqs. (20) and (21) for the displacements in the global coordinate system results in Eqs. (23) and (24):

$$\begin{Bmatrix} \delta_x \\ \delta_y \end{Bmatrix}^{(b1)} = \begin{bmatrix} S_{xx,b1} & -S_{xy,b1} \\ -S_{xy,b1} & S_{yy,b1} \end{bmatrix} \bullet \begin{Bmatrix} \mathrm{F_x} \\ \mathrm{F_y} \end{Bmatrix}^{(b1)} \tag{23}$$

$$\begin{Bmatrix} \delta_x \\ \delta_y \end{Bmatrix}^{(b2)} = \begin{bmatrix} S_{xx,b2} & -S_{xy,b2} \\ -S_{xy,b2} & S_{xx,b2} \end{bmatrix} \bullet \begin{Bmatrix} \mathrm{F_x} \\ \mathrm{F_y} \end{Bmatrix}^{(b2)} \tag{24}$$

The compliance terms in Eqs. (23) and (24) are given by the following expressions:

$$S_{xx,b1} = \frac{{s_{b1}}^2}{K_{v,b1}} + \frac{{c_{b1}}^2}{K_{ax,b1}}; S_{xx,b2} = \frac{{s_{b2}}^2}{K_{v,b2}} + \frac{{c_{b2}}^2}{K_{ax,b2}} \tag{25}$$

$$S_{yy,b1} = \frac{{c_{b1}}^2}{K_{v,b1}} + \frac{{s_{b1}}^2}{K_{ax,b1}}; S_{yy,b2} = \frac{{c_{b2}}^2}{K_{v,b2}} + \frac{{s_{b2}}^2}{K_{ax,b2}} \tag{26}$$

$$S_{xy,b1} = s_{b1} \bullet c_{b1} \bullet \left(\frac{1}{\mathrm{K_{v,b1}}} - \frac{1}{\mathrm{K_{ax,b1}}}\right); \mathrm{S_{xy,b2}} = \mathrm{s_{b2}} \bullet \mathrm{c_{b2}} \bullet \left(\frac{1}{\mathrm{K_{ax,b2}}} - \frac{1}{\mathrm{K_{v,b2}}}\right) \tag{27}$$

The forces at the tensile side (rod b_1) and the compressive side (rod b_2) per plane of rods are given by Eqs. (28) and (29), see also Eqs. (2) and (3) and Fig. 2(a):

$$\begin{Bmatrix} F_x \\ F_y \end{Bmatrix}^{(b1)} = \frac{1}{n} \bullet \begin{Bmatrix} \mathrm{M/z} \\ \mathrm{V/2} \end{Bmatrix} = \frac{1}{\mathrm{n}} \bullet \begin{Bmatrix} \mathrm{M/z} \\ \mathrm{M/(2 \bullet L_v)} \end{Bmatrix} \tag{28}$$

$$\begin{Bmatrix} F_x \\ F_y \end{Bmatrix}^{(b2)} = \frac{1}{n} \bullet \begin{Bmatrix} \mathrm{-M/z} \\ \mathrm{V/2} \end{Bmatrix} = \frac{1}{\mathrm{n}} \bullet \begin{Bmatrix} \mathrm{-M/z} \\ \mathrm{M/(2 \bullet L_v)} \end{Bmatrix} \tag{29}$$

The horizontal displacements are obtained by substituting Eqs. (28) and (29) into Eqs. (23) and (24):

$${\delta_x}^{(b1)} = \frac{1}{n} \bullet \left(\mathrm{S_{xx,b1}} \bullet \frac{\mathrm{M}}{\mathrm{z}} - \mathrm{S_{xy,b1}} \bullet \frac{\mathrm{M}}{\mathrm{2 \bullet L_v}}\right) \tag{30}$$

$${\delta_x}^{(b2)} = -\frac{1}{n} \bullet \left(\mathrm{S_{xx,b2}} \bullet \frac{\mathrm{M}}{\mathrm{z}} + \mathrm{S_{xy,b2}} \bullet \frac{\mathrm{M}}{\mathrm{2 \bullet L_v}}\right) \tag{31}$$

The rotation is given as function of the horizontal displacements, confer also Fig. 2(d):

$$\theta_b = \frac{{\delta_x}^{(b1)} - {\delta_x}^{(b2)}}{z} \tag{32}$$

Combining Eqs. (30) to (32), the rotational stiffness per plane of rods is obtained:

$$K_{\theta,b} = \frac{1}{n} \bullet \frac{\mathrm{M}}{\theta_\mathrm{b}} = \frac{\mathrm{z}^2}{\left(\mathrm{S_{xx,b1}} + \mathrm{S_{xx,b2}}\right) + \left(\mathrm{S_{xy,b2}} - \mathrm{S_{xy,b1}}\right) \bullet \frac{\mathrm{z}}{\mathrm{2 \bullet L_v}}} \tag{33}$$

Finally, the forces in the rods are given by Eqs. (34) and (35):

$$\begin{Bmatrix} F_{ax,b1} \\ F_{v,b1} \end{Bmatrix} = \left(\boldsymbol{Q_{b1}}^{T}\right)^{-1} \bullet \begin{Bmatrix} \mathrm{F_x} \\ \mathrm{F_y} \end{Bmatrix}^{(b1)} = \frac{1}{\mathrm{n}} \bullet \begin{Bmatrix} \mathrm{c_{b1}} + \mathrm{s_{b1}} \bullet \mathrm{z}/(2 \bullet \mathrm{L_v}) \\ -\mathrm{s_{b1}} + \mathrm{c_{b1}} \bullet \mathrm{z}/(2 \bullet \mathrm{L_v}) \end{Bmatrix} \bullet \frac{\mathrm{M}}{\mathrm{z}} \tag{34}$$

$$\begin{Bmatrix} F_{ax,b2} \\ F_{v,b2} \end{Bmatrix} = \left(\boldsymbol{Q_{b2}}^{T}\right)^{-1} \bullet \begin{Bmatrix} \mathrm{F_x} \\ \mathrm{F_y} \end{Bmatrix}^{(b2)} = -\frac{1}{\mathrm{n}} \bullet \begin{Bmatrix} \mathrm{c_{b2}} + \mathrm{s_{b2}} \bullet \mathrm{z}/(2 \bullet \mathrm{L_v}) \\ -\mathrm{s_{b2}} + \mathrm{c_{b2}} \bullet \mathrm{z}/(2 \bullet \mathrm{L_v}) \end{Bmatrix} \bullet \frac{\mathrm{M}}{\mathrm{z}} \tag{35}$$

3.2.3. Steel connectors

The steel rings are represented by spring components with spring constants $K_{ax,con,1}$ and $K_{ax,con,2}$, see also Fig. 2(e). Assuming linear elasticity, the rotational stiffness of the connectors is given by:

$$K_{\theta,con} = \frac{1}{n} \bullet \frac{\mathrm{M}}{\theta_\mathrm{con}} = \mathrm{z}^2 \bullet \left(\frac{1}{\mathrm{K_{ax,con,1}}} + \frac{1}{\mathrm{K_{ax,con,2}}}\right)^{-1} \tag{36}$$

3.2.4. Rotational stiffness of entire connection

The total deformation of the connection is obtained by adding the deformation in each part. This is equivalent to a system of rotational springs placed in series. Taking all sources of deformation into account, the rotational stiffness of the entire connection per plane of rods is given by Eq. (37):

$$K_{\theta,tot} = \left(\frac{1}{K_{\theta,c}} + \frac{1}{K_{\theta,b}} + \frac{1}{K_{\theta,con}}\right)^{-1} \tag{37}$$

3.3. Resistance considerations

3.3.1. Capacity of threaded rods and coupling parts

A power criterion is often used – as an approximation – to determine the capacity of fasteners subjected to combined axial force (F_{ax}) and lateral force (F_v), i.e.:

$$\left(\frac{F_{ax}}{F_{ax,R}}\right)^{q} + \left(\frac{F_v}{F_{v,R}}\right)^{q} \leq 1 \tag{38}$$

In Eq. (38), $F_{ax,R}$ and $F_{v,R}$ are the axial and lateral capacity of a fastener respectively. According to EN 1995-1-1 [14], a quadratic failure criterion applies for screws, i.e. $q = 2$. The quadratic failure criterion has provided safe-sided predictions for long self-tapping screws (i.e. with steel failure being more critical than withdrawal) inserted perpendicular to grain [15] and for glued-in rods parallel to grain [16].

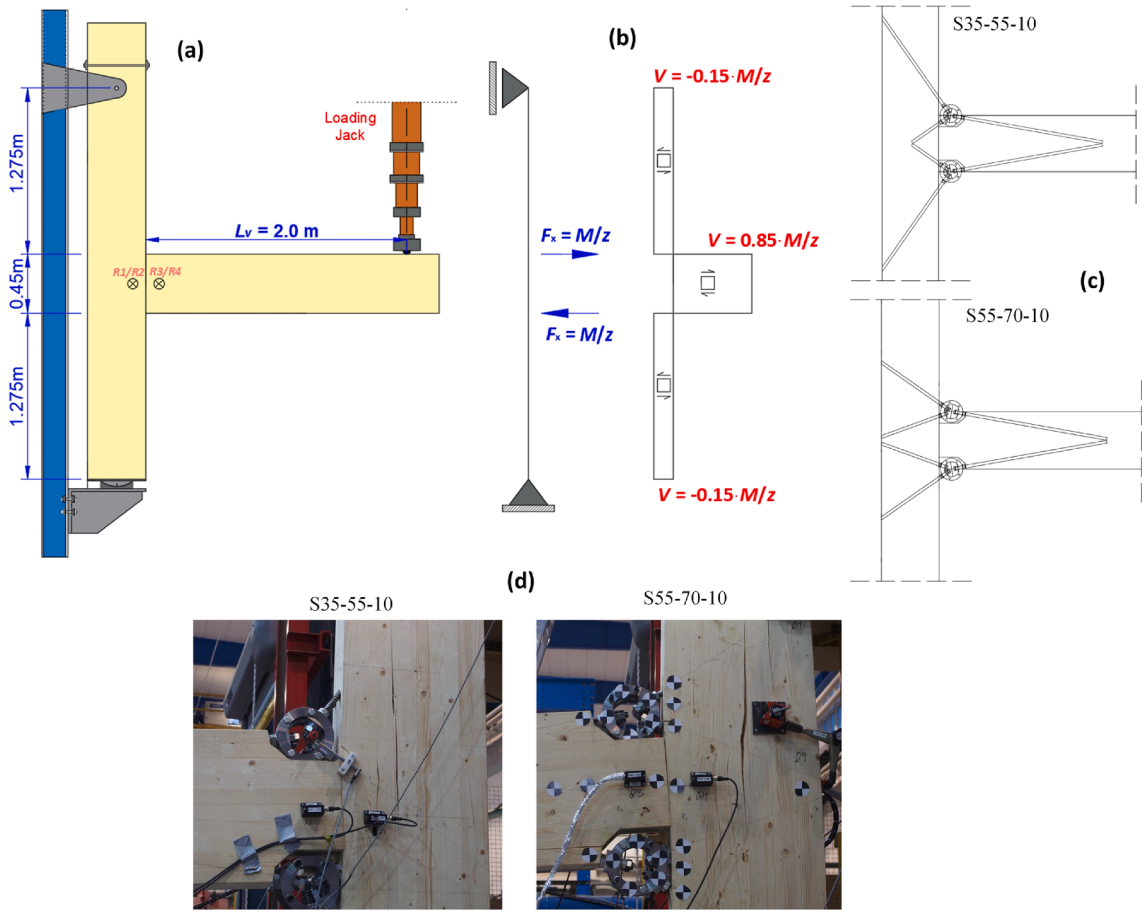

Fig. 3. Full-scale tests by Lied and Nordal [13]: (a) experimental set-up, (b) simplified static system and estimated shear forces in the column, (c) lay-out of specimens and (d) failure modes.

However, more experimental verification is required with respect to such failure criteria. The threaded rods in the column are mainly axially loaded (i.e. $F_{v,ci} \approx 0$) as explained in Section 2.2 and therefore in this case Eq. (38) reduces to:

$$\left|F_{ax,ci}\right| \leq F_{ax,R} \tag{39}$$

Finally, the steel coupling parts should have sufficient resistance.

3.3.2. *Failure in the panel zone of the column*

The application of horizontal forces results in high shear stresses in the panel zone of the column, i.e. the region between threaded rods c_1-c_2 and c_3-c_4. Moreover, stresses perpendicular to grain occur around the threaded rods. The combination of tensile stresses perpendicular to grain and shear stresses is unfavourable due to their high degree of interaction [17] and may cause fracture in the panel zone.

3.4. *Properties of threaded rods*

3.4.1. *Axially loaded threaded rods*

The properties of threaded rods are necessary inputs for the presented component method. Considering the withdrawal stiffness of a threaded rod under service load ($K_{ser,ax}$) and the stiffness of the free non-embedded part ($K_{ax,l0}$), the total axial stiffness of a threaded rod is given by:

$$K_{ax} = \frac{K_{ser,ax} \bullet K_{ax,l0}}{K_{ser,ax} + K_{ax,l0}} \tag{40}$$

Eq. (41) is an approximation for the withdrawal stiffness of a threaded rod [18] ($K_{ser,ax}$ in N/mm):

$$K_{ser,ax} \approx \frac{50000 \bullet (d/20)^2 \bullet (\rho_m/470)^2 \bullet \min\left[(l/300)^{0.75}, 1.0\right]}{0.40 \bullet \cos^{2.3}\alpha + \sin^{2.3}\alpha} \tag{41}$$

where d is the outer-thread diameter of the rod (in mm), l is the penetration length of the rod (in mm), ρ_m is the mean density of timber (in kg/m^3) and α is the angle between the rod and the grain direction. The axial stiffness of the non-embedded part is given by:

$$K_{ax,l0} = A_{net} \bullet \mathrm{E_s}/\mathrm{l_0} \tag{42}$$

where:

- $E_s = 210000$ N/mm^2 is the modulus of elasticity of steel
- $A_{net} \approx \pi \bullet \mathrm{d_{net}}^2/4$ is the net area of the rod (for rods with a metric-threaded end as shown in Fig. 1(c), d_{net} may be approximated as 90% of the diameter of the metric thread [19]);
- l_0 is the non-embedded length of the rod, i.e. the length between the fixing point of the rod in the coupling part and the entrance point of the thread in the timber, see also Fig. 2(a).

The axial capacity per threaded rod is given by Eq. (43):

Table 1
Parameters for tests in accordance with Fig. 3 [13]

Test	Parameters
S35-55–10	$\alpha_{c1} = \alpha_{c4} = 35^{\circ}$, $\alpha_{c2} = \alpha_{c3} = 55^{\circ}$, $\alpha_{b1} = \alpha_{b2} = 10^{\circ} l_{c1} = l_{c4} = 785$mm, $l_{c2} = l_{c3} = 240$mm, $l_{b1} = l_{b2} = 1100$mm$l_{0,c1}$ [a] $= 120$ mm, $l_{0,c2}$ [a] $= 80$ mm, $l_{0,c3}$ [a] $= 35$ mm, $l_{0,c4}$ [a] $= 75$ mm, $l_{0,b1}$ [a] $= 80$ mm, $l_{0,b2}$ a $= 35$ mmz $=$ 450mm, $L_v = 2000$ mm
S55-70–10	$\alpha_{c1} = \alpha_{c4} = 55^{\circ}$, $\alpha_{c2} = \alpha_{c3} = 70^{\circ}$, $\alpha_{b1} = \alpha_{b2} = 10^{\circ} l_{c1} = l_{c4} = 540$mm, $l_{c2} = l_{c3} = 450$mm, $l_{b1} = l_{b2} = 1100$mm$l_{0,c1}$ [a] $= 80$ mm, $l_{0,c2}$ [a] $= 95$ mm, $l_{0,c3}$ [a] $= 50$ mm, $l_{0,c4}$ [a] $= 35$ mm, $l_{0,b1}$ [a] $= 80$ mm, $l_{0,b2}$ a $= 35$ mmz $=$ 450mm, $L_v = 2000$ mm

[a] $l_{0,c1} \neq l_{0,c4}$, $l_{0,c2} \neq l_{0,c3}$ and $l_{0,b1} \neq l_{0,b2}$ despite geometric symmetry: the tensile loads in the top edge are transferred by contact between fixing nuts and the interior surface of the rings, while the compressive loads in the bottom edge are transferred by contact between fixing nuts and the exterior surface of the rings.

$$F_{ax,R} = \frac{n_{ef}}{n} \bullet \min \begin{Bmatrix} F_{ax,\alpha,R} \\ F_{tens,R} \end{Bmatrix} \tag{43}$$

where:

- $F_{ax,\alpha,R}$ is the withdrawal capacity per rod;
- $F_{tens,R}$ is the design tensile capacity of each rod;
- n is the number of threaded rods acting together (i.e. the plane of rods);
- n_{ef} is the effective number of rods acting together and according to EN1995-1-1 [14] it may be estimated as function of the number of planes of rods as:

$$n_{ef} = n^{0.9} \tag{44}$$

In [18], the following simplified expression for the mean withdrawal capacity is provided:

$$F_{ax,\alpha,Rm} \approx 15.0 \bullet d \bullet l \bullet (\rho_m/470) \tag{45}$$

On principle, the buckling resistance should also be verified for rods subjected to compressive forces.

3.4.2. *Laterally loaded threaded rods*

The lateral stiffness of the threaded rods is an input parameter for the determination of the properties of the beam-side connection as discussed in Section 3.2.2. Assuming that rotation of the rods is not allowed at the fixing points in the coupling parts (since rods are fastened by nuts on both sides of the rings), the total vertical stiffness (K_v) of a threaded rod can be estimated by Eq. (46) [18]:

$$\frac{K_v = 3 \bullet k_v \bullet l_{ch}}{\lambda_0^3 + 3 \bullet \lambda_0^2 + 3 \bullet \lambda_0 + 3} \tag{46}$$

The parameters λ_0 and l_{ch} have been defined as follows [18]:

$$\lambda_0 = l_0/l_{ch}; l_{ch} = \sqrt[4]{4} \bullet E_s \bullet I_s/k_v \tag{47}$$

The parameter $I_s \approx \pi \bullet d_1^4/64$ is the 2nd moment of area of the rod and d_1 is the core diameter. The parameter k_v is the foundation modulus (i.e. stiffness per unit length) of a laterally loaded rod.

The load-carrying capacity of a long, laterally-loaded rod, loaded with eccentricity l_0 is given by Eq. (48) [20]:

$$F_{v,R} = f_h \bullet d_{ef} \bullet \left(\sqrt{\frac{2 \bullet M_{y,R}}{f_h \bullet d_{ef}} + e_0^2} - e_0 \right) \tag{48}$$

where f_h is the embedment strength, $M_{y,R}$ is the yielding moment and d_{ef} is an effective diameter taking into account the presence of the thread. According to EN 1995-1-1 [14] the effective diameter is approximated as 1.1 times the core diameter, i.e. $d_{ef} = 1.1 \bullet d_1$. The value of e_0 depends on whether the rotation at the loading point is restrained or not: if rotation is allowed $e_0 = l_0$ and if rotation is restrained $e_0 = (l_0 - l_{ch})/2$ [18]. The latter is assumed to be more realistic because rods are fastened by nuts on both sides of the rings. The threaded rods are inserted with small inclination to the grain in the beam and therefore the foundation modulus k_v and the embedment strength f_h perpendicular to the grain may be used as approximations.

4. Experimental validation

In this Section, the analytical predictions according to the component method are compared to test results obtained by two experimental

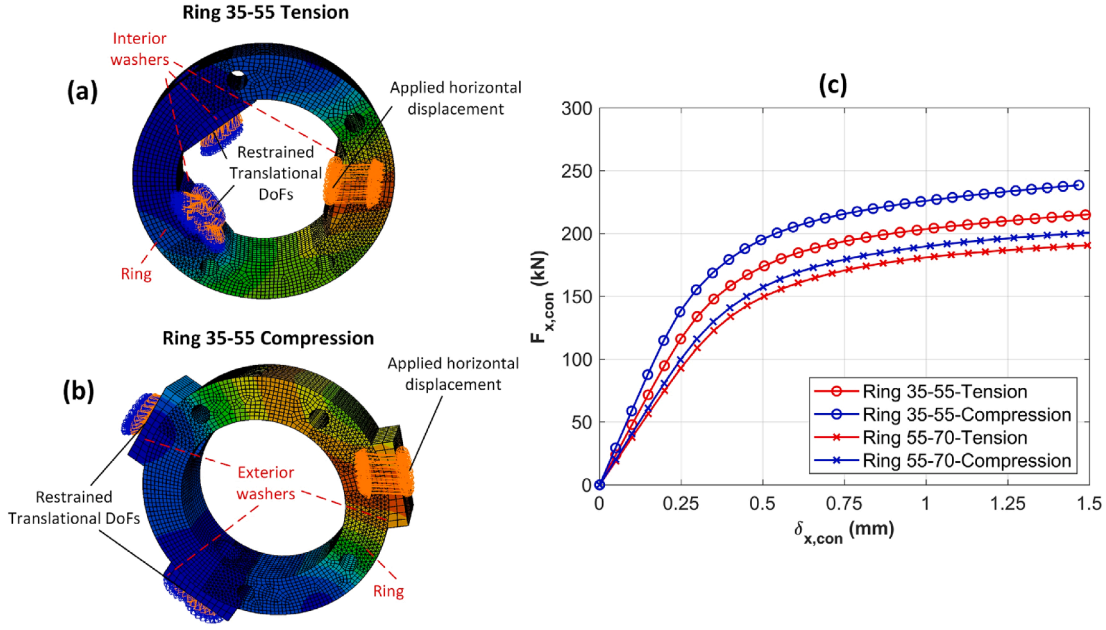

Fig. 4. FE simulations of steel rings: (a) Ring 35–55 in tension, (b) Ring 35–55 in compression, (c) Force-displacement curves for all cases.

Table 2
Material properties of S355 steel in FE model.

Material property	Values	
Modulus of elasticity	$E_s = 210000$ N/mm^2	
Poisson's ratio	$\nu = 0.30$	
Plastic strain levels at selected stress levels[25]	$\sigma = 311.0$N/mm^2	$\varepsilon_p = 0$
	$\sigma = 346.9$N/mm^2	$\varepsilon_p = 0.4\%$
	$\sigma = 355.9$N/mm^2	$\varepsilon_p = 1.97\%$
	$\sigma = 541.6$N/mm^2	$\varepsilon_p = 13.91\%$

Table 3
Tests with rings as coupling parts (Fig. 1 and Fig. 3) – Stiffness predictions vs experimental results.

Parameter	Units	Reference	S35-55–10	S55-70–10
$K_{ax,c1}$	(kN/mm)	Eq. (40) in parenthesis:	78.5 (95.3, 445.3)	61.8 (68.1, 668.0)
$K_{ax,c2}$			53.0 (57.6, 668.0)	51.1 (56.2, 562.5)
$K_{ax,c3}$			55.5 (57.6, 1526.8)	53.4 (56.2, 1068.8)
$K_{ax,c4}$		$K_{ser,ax}$, $K_{ax,l0}$ Eq. (41),Eq.(42)	84.0 (95.3, 712.5)	65.2 (68.1, 1526.8)
$K_{ax,b1}$			105.5 (125.4, 668.0)	105.5 (125.4, 668.0)
$K_{ax,b2}$			115.8 (125.4, 1526.8)	115.8 (125.4, 1526.8)
$K_{v,b1}$	(kN/mm)	Eq. (46)[a]	3.64[a]	3.64[a]
$K_{v,b2}$			9.05[a]	9.05[a]
$K_{ax,con,1}$	(kN/mm)	Fig. 4	484	381
$K_{ax,con,2}$			600	412
$K_{\theta,c}$ (per plane of rods)	(kNm/rad)	Eq. (17)	6291	8825
$K_{\theta,b}$ (per plane of rods)		Eq. (33)	9156	9156
$K_{\theta,con}$ (per plane of rods)		Eq. (36)	54,249	40,084
$K_{\theta,tot}$ (per plane of rods)		Eq. (37)	3489	4041
$K_{\theta,tot}$ (entire connection)	(kNm/rad)	Eq. (37): $n \cdot K_{\theta,tot}$	**6978**	**8082**
		Experimental [13]	**7120[b]**	**6579[b] (7541[c])**
Deviation between analytical predictions and test results			−2.0%	22.8 % (7.2% [c])

Input for calculations: $\rho_m = 430$ kg/m3, $d = 22$ mm; $d_1 = 16.1$ mm, $d_{net} = 0.9 \cdot 20 = 18$ mm, $n = 2$. $E_s = 210000$ N/mm2, $k_v \approx k_{v,90} = 300$ N/mm2 [26], $I_s = 3298$ mm4, $l_{ch} = 55.1$ mm (Eq. (47)).
a The vertical stiffness was calculated by the following more accurate form of Eq. (46) which takes into account the fact that the diameter in the free length is d_{net} but the core diameter of the embedded rod is d_1: $K_v = 3 \cdot m \cdot k_v \cdot l_{ch} \cdot (\lambda_0 + m)/(\lambda_0^4 + 4 \cdot \lambda_0^3 \cdot m + 6 \cdot \lambda_0^2 \cdot m + 6 \cdot \lambda_0 \cdot m + 3 \cdot m^2)$, $m = d_{net}^4/d_1^4$
Compared to Eq. (46) with d_1, this equation results in approx. 20% higher values of K_v, approx. 3% higher values in $K_{\theta,b}$ and approx. 1.5% higher values in $K_{\theta,tot}$ i.e. the use of Eq. (46) with d_1 would be a good approximation.
b Measurement based on two pairs of inclinometers attached on both sides of the beam and the column, see Fig. 1(d).
c Measurement based on digital image correlation.

series. In Section 4.1, test results from two prototype full-scale tests of moment-resisting, beam-to-column connections with steel rings as coupling parts [13] (as shown in Fig. 1(a)) are presented in detail and compared to the analytical predictions. In Section 4.2, test results from a similar prototype connection with a steel connector consisting of an IPE profile and welded steel plates [21] are briefly presented and compared to the analytical predictions.

Table 4
Tests with rings as coupling parts (Fig. 1 and Fig. 3) – Forces and utilization ratios at failure.

Parameter	Reference	S35-55–10	S55-70–10
Failure moment (test),M_u [13]	Fig. 3	**78.8 kNm**	**133.3 kNm**
Panel zone	Fig. 3		
$V_{u,column}$ [a]		165.6 kN	280.1 kN
$\tau_{v,u,column} = 1.5 \cdot V_{u,column}/b \cdot h$		3.94 N/mm^2	6.67 N/mm^2
Utilization ratios in each rod			
Axial load in rods (W: withdrawal / S:steel)			
$F_{ax,c1}/F_{ax,R,c1}$	Eq. (18)[1]/Eq. (43)	W:26.4%/ S:32.2%	W:53.2%/ S:44.8%
$F_{ax,c2}/F_{ax,R,c2}$	Eq. (18)[2]/Eq. (43)	W:97.7%/ S:36.5%	W:68.7%/ S:48.1%
$F_{ax,c3}/F_{ax,R,c3}$	Eq. (19)[1]/Eq. (43)	W:97.7%/ S:36.5%	W:68.7%/ S:48.1%
$F_{ax,c4}/F_{ax,R,c4}$	Eq. (19)[2]/Eq. (43)	W:26.4%/ S:32.2%	W:53.2%/ S:44.8%
$F_{ax,b1}/F_{ax,R,b1}$	Eq. (34)[1]/Eq. (43)	W:28.3%/ S:48.6%	W:48.0%/ S:82.3%
$F_{ax,b2}/F_{ax,R,b2}$	Eq. (35)[1]/Eq. (43)	W:28.3%/ S:48.6%	W:48.0%/ S:82.3%
Lateral load in rods			
$F_{v,b1}/F_{v,R,b1}$	Eq. (34)[2]/Eq. (48)	30.4%	51.4%
$F_{v,b2}/F_{v,R,b2}$	Eq. (35)[2] /Eq. (48)	22.2%	37.5%
Steel rings			
$F_x = F_{x,con}$ (per ring)	Eq. (2)	87.5 kN	148.1 kN

[a] Determined for the moment corresponding to the centroid of the column, i.e. $M_u = F_{jack,u} \cdot (2 + 0.225)$m.
Ultimate steel strength [13]: $f_{u,mean} = 952$ N/mm^2 $\rightarrow F_{tens,R} = A_s \cdot f_{u,mean} = (\pi \cdot 16.1^2/4) \cdot 952 \cdot 10^{-3}$ kN $= 193.8$ kN.
Mean embedment strength (for the same rods in GL30c) [26]: $f_h \approx f_{h,90} = 17.2$ N/mm^2, $d_{ef} = 1.1 \cdot d_1$.
Mean yielding moment of the rods [26]: $M_{y,R} = 7.63 \cdot 10^5$ N • mm.
Note: No buckling failures of the rods subjected to compression were observed in the tests [13]. The existing model for buckling of self-tapping screws [27] has not been verified for threaded rods.
[1,2] 1st and 2nd part of the equation respectively.

4.1. Connection with steel rings as coupling parts

The set-up for these tests [13] and the specimens are presented in Fig. 3. The specimens were tested according to EN 26891:1991 [22]. The beam and the column were made of Norway spruce glulam (*Picea Abies*) of strength class GL30c [23] with lamination thickness of 45 mm. The cross–sectional dimensions of both the beam and the column were $b \times h = 140 \times 450$ mm. The moisture content was approximately 12%. The beam and the column were assembled with a gap at their interface and therefore transfer of forces by contact was not allowed, at least for small values of moment. Purpose-made threaded rods with outer-thread diameter $d = 22$ mm, core diameter $d_1 = 16.1$ mm and metric M20 thread in one of their ends were used, see Fig. 1(c).

Two planes of rods were used (i.e. $n = 2$). The spacing and edge distances of rods, as specified in Fig. 1(b), were $a_2 = 60$ mm and $a_4 = 40$ mm. The tests are named $S_{ac1\text{-}ac2\text{-}ab1}$, based on the angles of the rods. The angles α_i, the embedment lengths l_i, and the free lengths of the rods $l_{0,i}$ of the rods for each test are given in Table 1.

Steel rings (Fig. 1(d)) of steel quality S355 with an inner diameter of 115.2 mm and an outer diameter of 172.3 mm were used. Holes with diameter 22 mm were drilled to allow the mounting of threaded rods at their metric-threaded end, i.e. a small tolerance of 2 mm was provided to allow for easy assembly. Afterwards, the part was sliced in the symmetry

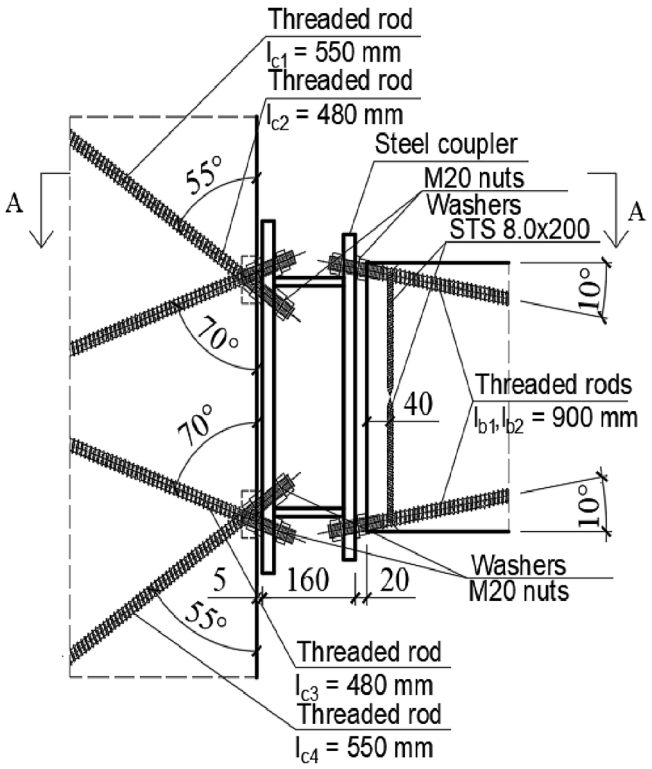

Fig. 5. Details of connection details with steel connector [21]

line resulting in two connecting parts, which could be wrapped and clamped around the rods, and fastened together with bolts (Fig. 1(d)).

In order to evaluate the stiffness and the resistance of the rings, simplified 3D Finite Element (abbr. FE) simulations were carried out by use of Abaqus software [24]. FE simulations were carried for the rings used in each test (Ring35-55 for test S35-55-10 and Ring55-70 for test S55-70-10), both for tensile and compressive loading. The FE models for Ring35-55 are given as an example in Fig. 4(a and b). As a simplification, the washers were assumed tied to the ring. Moreover, the ring was modelled as a whole part, i.e. the slicing of the ring about its symmetry line as shown in Fig. 1(d) was disregarded in the FE models. The rings and the washers were meshed with 8-node, linear, steel, brick elements. The material properties of steel for the FE models are given in Table 2. The plasticity of steel was taken into account by use of the stress-plastic strain levels given in Table 2 for S355 [25]. On the column side, the washers were assumed translationally restrained in the nodes that were in contact with the nuts (the nuts were not included in the model). On the beam side, the washers were subjected to monotonic horizontal displacement applied also in the contact nodes with the nuts. The force-displacement curves of the rings according to the FE results are summarized in Fig. 4(c). The elastic stiffness values with respect to horizontal displacement are $K_{ax,con,1}$ = 484 kN/mm (tension) and $K_{ax,con,2}$ = 600 kN/mm (compression) for Ring35-55, and $K_{ax,con,1}$ = 381 kN/mm (tension) and $K_{ax,con,2}$ = 412 kN/mm (compression) for Ring55-70.

Table 3 presents in detail the analytical predictions of the component method with respect to the rotational stiffness. The analytical predictions are in good agreement with the experimental results; they slightly underestimate the rotational stiffness for test S35-55-10 and they slightly overestimate the rotational stiffness for test S55-70-10 (in this case the stiffness was also measured by use of digital image correlation, giving a slightly higher value than the one based on inclinometers).

The analytical predictions for the shear stresses in the column and the utilization ratios in the rods are summarized in Table 4. The failure moments were 78.8 kNm and 133.3 kNm for tests S35-55-10 and S55-70-10, respectively. Both specimens failed due to fracture in the panel zone of the column (Fig. 3(d)) as a result of combined shear and tensile stresses perpendicular to grain acting in the panel zone. The influence of tensile stresses perpendicular to grain may be identified by the fact that fracture initiated in the upper part of the panel zone in which threaded rods were subjected to tensile loads. On the contrary, crack opening is prevented in the lower part of the panel zone due to the presence of compressive stresses.

The shear forces in the column can be estimated by the simplified shear force diagram in Fig. 3(b). Here, the lever arm to the centroid of the column was used to determine the shear force in the column. In test S35-55-10 the estimated shear stress in the column at failure was 3.94 N/mm^2, i.e. lower compared to the mean shear strength of spruce glulam [28]. This may be explained by the occurrence of high concentrations of tensile stresses perpendicular to grain at the tip of rods c_2 and c_3 (note that the tips of rods c_2 and c_3 are very close to the centroid of the column, i.e. at the theoretical position of maximum shear stress). In test S55-70-10, the estimated shear stress in the column at failure was 6.67 N/mm^2, i.e. significantly higher than test S35-55-10. This increased strength may be explained by the fact that rods are continuous in this case and they may act as reinforcements [29], especially for rods c_1 and c_2 which are located in the upper part of the panel zone which was subjected to tension.

Table 4 also presents the estimated utilization ratios of all rods at failure. At the column side, all estimated axial forces in the rods (Eqs. (18) and (19)) were smaller than the corresponding axial capacities (Eq.

Table 5
Connection with steel connector (Fig. 5) –Stiffness predictions vs experimental results.

	Stiffness per plane of rods			Entire connection
Parameter	$K_{\theta,c}$ (kNm/rad)	$K_{\theta,b}$ (kNm/rad)	$K_{\theta,tot}$ (kNm/rad)	n•$K_{\theta,tot}$ (kNm/rad)
Analytical Predictions [a]	6353 (Eq. (17))	7820 (Eq. (33))	3358[b] (Eq. (37))	6716 (n = 2)
Mean Experimental results [c,d] [21]	6395 [d] (5 tests)	8720 (3 reinforced beams)8125 (2 unreinforced beams)	3809 (3 reinforced beams)3060 (2 unreinforced beams)3510(All 5 tests)	7618 (3 reinforced beams)6120(2 unreinforced beams)7020(All 5 tests)

[a] Test parameters, input for calculation [21], confer also Fig. 2(a) and Fig. 5. $\alpha_{c1} = \alpha_{c4} = 55^{\circ}$, $\alpha_{c2} = \alpha_{c3} = 70^{\circ}$, $l_{c1} = l_{c4} = 550$ mm, $l_{c2} = l_{c3} = 480$ mm, $l_{b1} = l_{b2} = 900$ mm. $l_{0,c1} = 65$ mm, $l_{0,c2} = 50$ mm, $l_{0,c3} = 30$ mm, $l_{0,c4} = 40$ mm, $l_{0,b1} = 45$ mm, $l_{0,b2} = 25$ mm. $z_c = 380$ mm, $z_b = 405$ mm, $L_v = 2300$ mm, Beam and column GL30c [23]: $\rho_m = 430$ kg/m^3, $MC \approx 12\%$. Threaded rods: the same as in Section 4.1.

[b] Input for calculation [21]: $K_{\theta,con} = 160000$ kNm/rad (entire connection), based on linear elastic FE analysis.

[c] Rotations obtained by use of displacement transducers placed on the top and the bottom of the connection on both sides.

[d] Based on all 5 tests:$CoV(K_{\theta,c}) = 18.0\%$, $CoV(K_{\theta,b}) = 9.8\%$, $CoV(K_{\theta,tot}) = 13.5\%$.

(43)). At the beam side (rods b_1-b_2), the estimated axial forces and lateral forces (Eqs. (34) and (35)) were smaller than the corresponding capacities (Eq. (43) and Eq. (48)) and moreover the quadratic failure criterion (Eq. (38), with $q = 2$) was satisfied. Finally, the axial forces in the rings at failure are also given in Table 4. For test S35-55-10 the axial force (87.5 kN) was well within the elastic range and for test S55-70-10, the axial force (148.1 kN) would result in very limited plastic behaviour in the rings, confer Fig. 4(c). No visible plastic deformation was observed after the tests.

4.2. Connection with steel connector consisting of an IPE profile and welded plates

Another prototype [21] of a connection with inclined threaded rods constructed according to the principle in Fig. 1 is presented in Fig. 5. In this prototype, the coupling part is a steel connector consisting of an IPE profile and welded plates instead of the steel rings. In the experimental campaign for this prototype [21] five specimens were tested. Five different columns ($b \times h = 200 \times 450$ mm^2) and five different beams ($b \times h = 140 \times 405$ mm^2) of strength class GL30c [23] were used in these tests. The arrangement of the rods was identical for all experiments. Three of the beams were reinforced with two 8-mm self-tapping screws inserted perpendicular to the grain (in the vertical direction), see Fig. 5. The other two beams were not reinforced.

Table 5 presents the input parameters and the experimental results for the mean rotational stiffness obtained by static monotonic testing according to EN 26891:1991 [22], together with the corresponding analytical predictions. In this series, additional deformation measurements were taken for the beam-side and the column-side, allowing comparison between the analytical predictions and the experimental results in each part. As shown in Table 5, the analytical predictions for the rotational stiffness are in very good agreement with the test results, both in terms of total stiffness as well as stiffness per part (column-side, beam-side).

All specimens failed due to splitting of the beam in both planes perpendicular to the grain [21]. Therefore, no conclusion can be reached with respect to the load-carrying capacity of the rods, according to Eqs. (38) and (39). At failure, the utilization ratios of the rods were significantly smaller than one, both in the column (see Eq. (39)) and in the beam (see Eq. (38), assuming $q = 2$).

5. Concluding remarks

Semi-rigid, moment-resisting connections can enhance the performance of multi-storey timber buildings. At present, such connections are not very common in practice. In this paper, a structural concept for a moment-resisting beam-to-column timber connection with inclined screwed-in threaded rods and metallic coupling parts was presented and explained. In this concept, threaded rods are mainly axially loaded to take advantage of their high axial capacity and stiffness. The reliable prediction of the rotational stiffness and the forces in the rods are necessary inputs in the analysis and the design process. A component method approach was developed for the analytical prediction of the rotational stiffness by simple analytical expressions. The analytical predictions for stiffness were compared with experimental results showing good agreement. Moreover, the component method can be used to estimate the forces in the rods at failure. Due to the variety of failure modes and limited test results, more test results are required to fully validate the failure criteria.

Declaration of Competing Interest

The authors declare that they have no known competing financial interests or personal relationships that could have appeared to influence the work reported in this paper.

Acknowledgements

The financial support by the Research Council of Norway, Norway through WoodSols project (NFR grant no. 254699/E50) is gratefully acknowledged.

Appendix A:. Parametric study

This Appendix presents a parametric study based on the derived analytical predictions in Section 3. Test S55-7010 is used as reference (see Section 4.1). The rods in the column are assumed continuous, e.g. as in the lay-out of connection in test S55-70-10. For varying angles, the penetration length and the free length of each rod are determined by geometry and angle of each rod. The lever arm is $L_v = M/V = 2000$ mm.

Fig. A.1(a) shows the analytical predictions for the rotational stiffness (per plane of rods) of the connection at the column-side according to Eq. (17) for varying angles of the rods. Symmetry of the angles is assumed, i.e. $a_{c1} = a_{c4}$ and $a_{c2} = a_{c3}$. As shown in Fig. A.1(a), the stiffness increases for increasing angles. However, greater angles result in practical implications due to the lack of space for nuts and washers (see e.g. Fig. 1(d)) and the lack of space for rods in the column.

Fig. A.1(b), shows the utilization of the rods with respect to withdrawal failure (i.e. Eqs. (18) and (19)) divided by the first term in Eq. (43)) for the failure moment in test S55-70 (i.e. $M_u = 133.3$ kNm). As shown in Fig. A.1(b), if rods c_1-c_4 and c_2-c_3 are inserted in similar angles, their utilization ratio is similar, and this configuration is optimal because the rods tend to share the load equally.

Fig. A.1(c) shows the effect of the lever arm L_v on the rotational stiffness at the column-side (Eq. (17)), at the beam-side (Eq. (33)) and the entire connection (Eq. (37)). The effect of the lever arm is greater on the beam-side stiffness. The influence decreases as the lever arm increases.

Fig. A.1(d) shows the influence of the angle of the rods at the beam-side (assuming $a_{b1} = a_{b2}$) for $L_v = 2000$ mm and $L_v = \infty$ (zero shear). The stiffness decreases significantly as the angle increases. Rods at the beam-side should be inclined as explained in Section 2.3. The angle should be small to maximize the stiffness.

Fig. A.1(e) shows and the influence of the lateral stiffness of wood (in terms of the foundation modulus k_v) on the stiffness at the beam-side. A moderate influence on the stiffness is observed for small values of k_v ($k_v \leq 500$–1000 N/mm^2). Finally, Fig. A.1(f) shows the influence of the lever arm z on the rotational stiffness. As indicated by the equations in Section 3.2 the stiffness is approximately proportional to z^2.

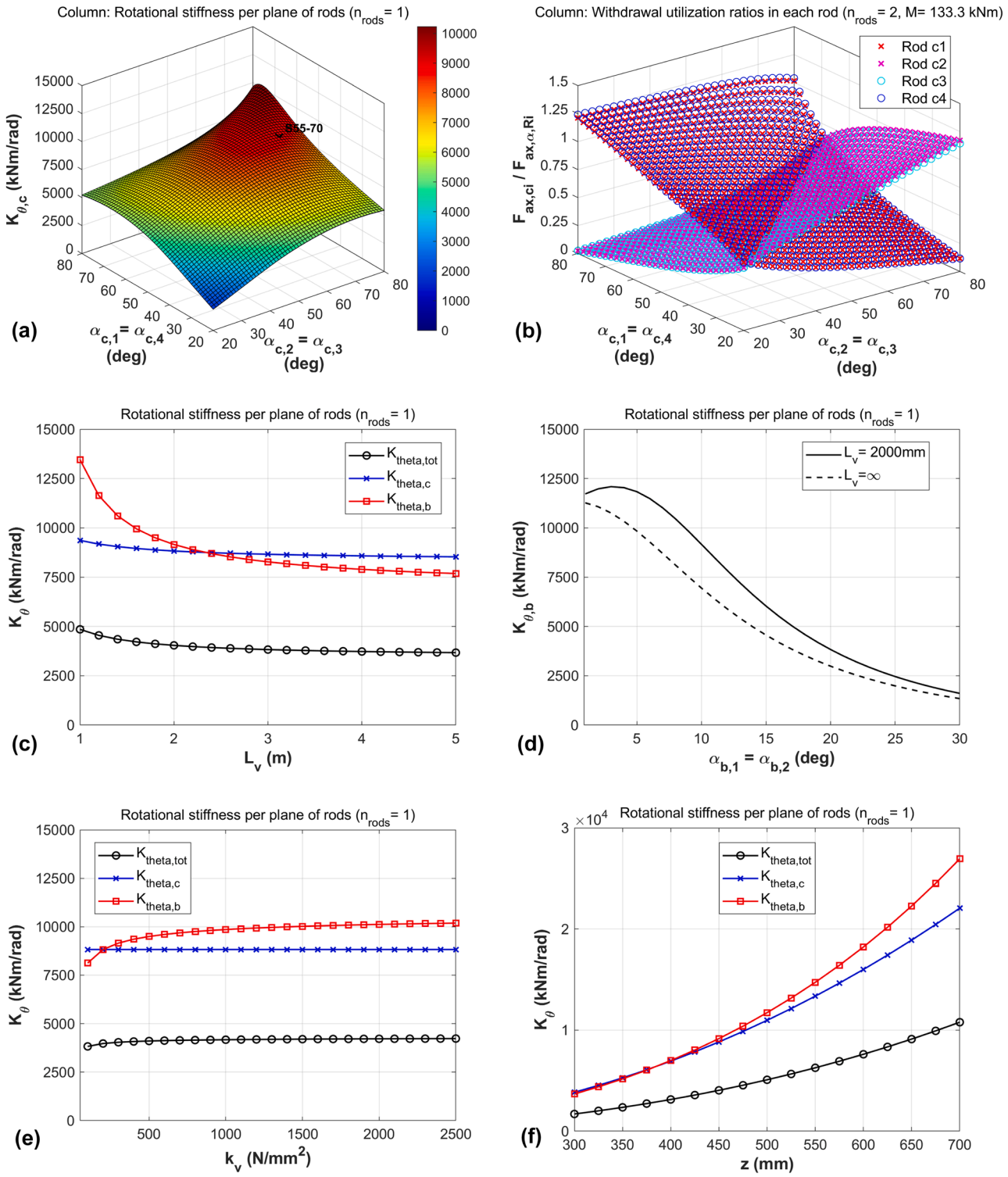

Fig. A1. Parametric study: (a) Column-side rotational stiffness per plane of rods (Eq. (17)) for varying rods' angles, (b) Utilization ratio (withdrawal failure) in rods at the column for varying rods' angles; Rotational stiffness per plane of rods as function of: the lever arm (c), as function of the rods' angle in the beam (d), as function of the lateral stiffness in the wood (e) and as function of the lever arm z (f).

References

[1] Stamatopoulos, H. and K.A. Malo. Wood frame solutions for free space design in urban buildings (WOODSOL) in 7th Forum Wood Building Nordic 2018. Växjö, Sweden.

[2] A. Vilguts, H. Stamatopoulos, K.A. Malo, Parametric analyses and feasibility study of moment-resisting timber frames under service load, Engineering Structures 228 (2021), 111583.

[3] Malo, K.A. and H. Stamatopoulos, *Connections with threaded rods in moment resisting frames*, in *Proceedings of the World Conference on Timber Engineering (WCTE 2016), August 22-25, 2016*, W.W. J. Eberhardsteiner, A. Fadai, M. Pöll, Editor. 2016, Vienna University of Technology, Austria, ISBN: 978-3-903039-00-1: Vienna, Austria.

[4] Malo, K.A. and J. Köhler. Vibrations of timber floor beams with end restraints. in Structures and Architecture: Concepts, Applications and Challenges – Proceedings

of the 2nd International Conference on Structures and Architecture, ICSA 2013. 2013.
[5] K. Komatsu, Q. Teng, Z. Li, X. Zhang, Z. Que, Experimental and analytical investigation on the nonlinear behaviors of glulam moment-resisting joints composed of inclined self-tapping screws with steel side plates, Advances in Structural Engineering 22 (15) (2019) 3190–3206.
[6] Closen, M. and F. Lam, Performance of moment resisting self-tapping screw assembly under reverse cyclic load, in Proceedings of the 12th World Conference on Timber Engineering. 2012: Auckland, New Zealand. p. 433-440.
[7] B. Kasal, P. Guindos, T. Polocoser, A. Heiduschke, S. Urushadze, S. Pospisil, Heavy laminated timber frames with rigid three-dimensional beam-to-column connections, Journal of Performance of Constructed Facilities 28 (6) (2014), https://doi.org/10.1061/(ASCE)CF.1943-5509.0000594.
[8] Andreolli, M., et al., *Ductile moment-resistant steel-timber connections.* Proceedings of the Institution of Civil Engineers: Structures and Buildings, 2011. **164**(2): p. 65-78.
[9] H. Yang, W. Liu, X. Ren, A component method for moment-resistant glulam beam–column connections with glued-in steel rods, Engineering Structures 115 (2016) 42–54.
[10] J. Ogrizovic, F. Wanninger, A. Frangi, Experimental and analytical analysis of moment-resisting connections with glued-in rods, Engineering Structures 145 (2017) 322–332.
[11] H. Stamatopoulos, K.A. Malo, Withdrawal capacity of threaded rods embedded in timber elements, Construction and Building Materials 94 (2015) 387–397.
[12] H. Stamatopoulos, K.A. Malo, Withdrawal stiffness of threaded rods embedded in timber elements, Construction and Building Materials 116 (2016) 263–272.
[13] Lied, K. and K. Nordal, *A conceptual study of glulam connections using threaded rods and connecting circular steel profiles*, in *Master thesis*. 2016, NTNU Norwegian University of Science and Technology: Trondheim, Norway.
[14] CEN, *NS-EN 1995-1-1:2004+A1:2008+A2:2014+NA:2010*, in *Design of timber structures – Part 1-1: General – Common rules and rules for buildings*. European committee for standarization: Brussels.
[15] Laggner, T., G. Flatscher, and G. Schickhofer, *Combined loading of self-tapping screws*, in *Proceedings of WCTE 2016 – World Conference on Timber Engineering*. 2016: Vienna, Austria.
[16] Aicher, S. and K. Simon, *Rigid Glulam Joints with Glued-in Rods subjected to Axial and Lateral Force Action*, in *Proceedings of the 8th INTER meeting* 2021: Karlsruher Institut für Technologie (KIT).
[17] Steiger, R. and E. Gehri, *Interaction of shear stresses and stresses perpendicular to grain*, in *Proceedings of the 44th CIB-W18 meeting* 2011: Alghero, Italy.
[18] H. Stamatopoulos, K.A. Malo, On strength and stiffness of screwed-in threaded rods embedded in softwood, Construction and Building Materials 261 (2020), 119999.
[19] CEN, *NS-EN 1993-1-8:2005+NA:2009*, in *Design of steel structures – Part 1-8: Design of joints*. 2009, European Committee for Standardization.
[20] Riberholt, H., *Glued bolts in glulam – Proposals for CIB code*, in *Proceedings of the 21st CIB-W18 meeting* 1988: Parksville, Canada.
[21] A. Vilguts, *Moment-resisting timber frames with semi-rigid connections*, in *Department of Structural Engineering*, Norwegian University of Science and Technology, Trondheim, Norway, 2021.
[22] CEN, *EN 26891:1991 (ISO 6891:1983): Timber structures- Joints made with mechanical fasteners-General principles for the determination of strength and deformation characteristics*. 1991, European Committee for Standardization: Brussels, Belgium.
[23] CEN, *EN 14080-2013: Timber structures- Glued laminated timber and glued solid timber – Requirements*. 2013, European Committee for Standardization: Brussels, Belgium.
[24] Simulia, *Abaqus analysis user's guide, Version 6.21*.
[25] DET NORSKE VERITAS AS, Determination of Structural Capacity by Non-linear FE analysis Methods, Recommended Practice DNV-RP-C208. 2013.
[26] H. Stamatopoulos, F.M. Massaro, J. Qazi, Mechanical properties of laterally loaded threaded rods embedded in softwood, European Journal of Wood and Wood Products (2021).
[27] Blaß, H.J. and I. Bejtka, *Reinforcements perpendicular to grain using self-tapping screws*, in *Proceedings of the 8th World Conference on Timber Engineering*. 2004: Lahti, Finland. p. 233-238.
[28] Sigbjørnsem, L., *Shear Properties of Nordic Glulam CE L40c*. 2012, Norwegian University of Science and Technology: Trondheim, Norway.
[29] Dietsch, P., H. Kreuzinger, and S. Winter, *Design of shear reinforcement for timber beams*, in *Proceedings of the 46th CIB-W18 meeting* 2013: Vancouver, Canada. p. 193-209.